Journal of Advanced Research in Numerical Heat Transfer

Journal homepage:
https://semarakilmu.com.my/journals/index.php/arnht/index
ISSN: 2735-0142

Numerical Investigation of Nanofluid-based Flow Behavior and Convective Heat Transfer Using Helical Screw

Abdulqader Salah Khlewee[1], Yaser Alaiwi[1], Talib Abdulameer Jasim[2], Mohammed Alamin Talib Mahdi[3], Abdullah Jabar Hussain[4], Zainab Al-Khafaji[5,6,*]

[1] Department of Mechanical Engineering, Altinbas University, Istanbul 34217, Turkey
[2] Department of Aeronautical Technical Engineering, College of Technical Engineering, Al-Farahidi University, Baghdad, Iraq
[3] Mechanical Engineering Department, University of Technology, Iraq
[4] Computer Techniques Engineering Department, College of Engineering and Engineering Techniques, Al-Mustaqbal University, 51001, Babylon, Iraq
[5] Department of Civil Engineering, Faculty of Engineering and Built Environment, Universiti Kebangsaan Malaysia, 43600 UKM Bangi, Selangor, Malaysia
[6] Scientific Research Center, Al-Ayen University, Thi-Qar, 64001, Iraq

ARTICLE INFO

Article history:
Received 10 August 2024
Received in revised form 13 September 2024
Accepted 14 October 2024
Available online 30 November 2024

Keywords:
Nanofluid; Flow Behavior; Convective heat transfer; Helical Screw; Tortional turbulator

ABSTRACT

A multitude of industrial and residential customers have utilized heat transfer devices for heat conversion and recovery. For the last fifty years, engineers have diligently endeavored to refine a heat exchanger design that reduces energy use without compromising efficiency. Most techniques for enhancing heat transfer operate by either augmenting the effective heat transfer surface area or inducing turbulence, hence reducing thermal resistance. This work utilized CFD to model Al2O3 and CuO nanoparticles inside the adsorber tube of a parabolic solar collector with N=1 and N=2 turbulators at Re of 20000, 60000, and 100000, respectively, with a turbulence intensity of 5%. The turbulence intensity was determined to be 5% of the total energy of the particles. The inclusion of nanoparticles in the base fluid enhances heat conduction. Consequently, nanofluids are viable options for alternate heat transmission mechanisms. Torsional turbulator models with N=2 have a higher output temperature (Temp) than those with N=1 due to the elevated practical heat level of the N=2 models. The intake temp is elevated from 35 to 46 degrees Celsius due to the existence of CuO nanoparticles in the adjacent turbulator adsorber tubes. The Reynolds number (Re) consistently increases the Nusselt number (Nu). Furthermore, the Nu indicates a higher quantity of CuO nanoparticle models compared to Al2O3 nanoparticle models. Furthermore, CuO nanoparticles exhibit superior efficacy compared to Al2O3 in pressure reduction. In comparison to the N=2 dual-turbulator mode, the N=1 single-turbulator mode exhibits a 34% increase in conflict. Pressure loss coefficients are higher for devices including two turbulators. Across a broad spectrum of Re, the thermal PEC for N=2 models exceeded that of N=1 models by 12 percentage points. CuO nanofluid receivers have better efficacy compared to Al2O3 receivers in the conversion of solar energy into thermal energy. The two-turbulator model, operating at a Re of 100000 and using CuO nanoparticles, attains optimal thermal

* *Corresponding author.*
E-mail address: p123005@siswa.ukm.edu.my (Zainab Al-Khafaji)

https://doi.org/10.37934/arnht.27.1.85106

efficiency. The factor of friction decreases with increasing Re, with Water N=1 showing higher frictional losses than Water N=2, indicating greater turbulence and resistance.

1. Introduction

Over the course of several decades, the proliferation of vortex/swirl flow devices for the purpose of attaining thermal systems with exceptional performance has experienced significant growth. Vortex/swirl flow devices, commonly referred to as insert devices, such as delta wings/winglets [1], twisted tapes [2], louvered strips [3], helical screws [4], and wire coils [5], were subjected to experimental and numerical analysis in order to identify the key variables that substantially enhance performance. An improved insertion apparatus should possess the capability to enhance convective heat transfer, thereby increasing the rate of heat transfer, while maintaining a tolerable pressure drop (minimizing factor of friction). However, in the case of various insert devices, their behavior with respect to heat transfer and flow mechanism is contingent upon their parameter design. During this phase, it will be imperative to meticulously choose appropriate geometries to maximize the likelihood of successfully attaining the desired objectives.

To maximize the thermal efficiency of thermal devices, a multitude of improved heat transfer methods were implemented for these devices. The techniques utilized for augmenting heat transfer involve the alteration of fluid transport features and flow features of the working fluid. The desired outcome can be attained by incorporating nanoparticle additives into the primary fluid and subsequently guiding the fluid flow through a curved conduit. Curved tubes have been widely employed in a multitude of applications. The spirally coiled tubing has been the subject of continuous and highly efficient investigations carried out by Naphon *et al.,* [6,7]. The investigation focused on the heat transfer and flow behaviors of water and nanofluids within a spirally coiled tube, considering various curvature ratios. The researchers further examined the effects of pulsating flow and magnetic field on the augmentation of heat transfer in spirally coiled tubes.

Nevertheless, numerous scholarly articles have elucidated the intricate intricacies of heat transfer and fluid dynamics, as well as the thermal efficiency of helically coiled tube heat exchangers. These investigations have explored a range of configurations, employing water and diverse nanofluids as the operational fluids [8-12]. Behabadi *et al.,* [12] performed an experimental investigation on the convective heat transfer features of nanofluids flowing through vertically helically coiled tubes with various configurations, while ensuring the maintenance of uniform wall temp conditions. Consideration has been given to the impact of Re, Dean number, geometrical parameters, and nanofluid weight fractions on the heat transfer and flow features of the coolant as it traverses the tube. Narreina and Mohammed [8] performed an inquiry into the influence of nanofluids and rotational motion on the heat transfer and fluid flow features within a helically coiled tube heat exchanger. In the investigation conducted by Darzi *et al.*, [13], a two-phase approach model was utilized to examine the turbulent heat transfer features of Al2O3-water nanofluids flowing through helically corrugated tubes.

A multitude of experimental investigations have been conducted by Jaisankar *et al.,* [14-16] to analyze the factor of friction and heat transfer features of thermosiphon solar water heating systems equipped with diverse configurations of twisted tapes. These configurations include twisted helical tapes, left–right twisted tapes with a spacer at the trailing edges, and left–right helical twisted tapes. The effects of Re and twist ratio were considered, and empirical correlations for factor of friction (f) and Nu were also obtained. The factor of friction features and heat transfer of circular tubes were subjected to experimental testing by Sivashanmugam *et al.,* [17,18]. The experiments involved the utilization of helical screw tape inserts to investigate both turbulent and laminar flow conditions. The

dimensions of the spacer, the torsional displacement, and the contribution of the right-left helical twist length were considered. Additionally, empirical relationships for the factor of friction (f) and Nu were established. Shekholeslami *et al.,* [19] investigated the heat transfer of nanofluids in a heat exchanger with a helical twisted tape using the Finite Volume Method. The findings demonstrated that an increase in the width ratio led to a decrease in the thickness of the thermal boundary layer due to the enhanced secondary flow strength.

Zhang *et al.,* [20] conducted a numerical investigation on the impact of helical screw tape inserts with various widths on flow friction and heat transfer coefficient. The experimental findings suggest a substantial increase in the factor of friction within plain circular tubes when equipped with helical screw tapes, ranging from 212% to 351%. Correspondingly, the heat transfer coefficient experienced a notable enhancement, ranging from 33% to 1020%. Hasanpour *et al.,* [21] conducted an experimental investigation on the factor of friction and heat transfer features of an inner corrugated tube equipped with various types of twisted tapes. The study examined both conventional and enhanced designs. The experimental findings indicate that the utilization of enhanced twisted tapes with corrugated tubes resulted in elevated magnitudes of f and Nu compared to the utilization of regular tapes.

The research gap identified in the existing literature highlights the need for a comprehensive understanding of the performance of vortex/swirl flow devices, particularly in relation to their design parameters and heat transfer capabilities. While numerous studies have explored the heat transfer and fluid dynamics of various insert devices, such as twisted tapes, helical screws, and delta wings, there remains a lack of focused investigation into the specific interactions between nanoparticle-enhanced nanofluids and the geometric configurations of these devices. Although advancements have been made in the use of nanofluids in curved conduits, the influence of various nanoparticle types on the heat transfer efficiency and pressure drop in complex flow scenarios, particularly within helically coiled tubes and under varying Reynolds number (Re), has not been fully addressed. Furthermore, existing research predominantly utilizes conventional nanofluids, and there is limited exploration into the potential of emerging nanofluids, such as those incorporating CuO or Al2O3, in optimizing thermal performance. Therefore, this study aims to fill this gap by systematically investigating the thermal and hydrodynamic performance of CuO and Al2O3 nanofluids in conjunction with innovative helical screw designs under a range of operating conditions, thereby contributing valuable insights to the field of thermal engineering and enhancing the design of future heat transfer systems. The model presented in the study on offers valuable applications across several domains within mechanical engineering. It can be employed to optimize the design of advanced heat exchangers in industrial processes, such as chemical manufacturing and power generation, where enhanced heat transfer rates can significantly improve energy efficiency. Furthermore, the insights derived from this model can inform the development of sophisticated cooling systems for electronic components, ensuring optimal thermal management and reliability. In solar thermal applications, the findings can contribute to designing systems that utilize nanofluids to enhance heat absorption and overall efficiency in energy conversion. Additionally, the model can be utilized to optimize heating, ventilation, and air conditioning (HVAC) systems by integrating nanofluids to enhance thermal performance while reducing energy consumption. The implications extend to renewable energy technologies, automotive cooling systems, and manufacturing processes, where effective heat transfer is critical for operational efficiency and product quality. Overall, the research provides a robust framework for leveraging nanofluid-based systems to enhance thermal performance and energy efficiency across diverse engineering applications. The aim of the current study is to investigate the heat transfer performance and flow behavior of nanofluids, specifically focusing on aluminum oxide (Al2O3) and copper oxide (CuO) nanoparticles, within the

adsorber tubes of a parabolic solar collector. This study seeks to evaluate the impact of various turbulators (N=1 and N=2) on the thermal efficiency and overall heat conversion capabilities of the system under varying Re (Re = 20000, 60000, and 100000) and a defined turbulence strength. By employing computational fluid dynamics (CFD) simulations, the research aims to elucidate the comparative advantages of CuO and Al2O3 nanofluids in enhancing heat conduction, reducing pressure losses, and optimizing the operational performance of solar thermal systems. Ultimately, the study aspires to provide valuable insights into the potential of nanofluids as effective heat transfer mediums in renewable energy applications.

2. Numerical Model

The researchers noted that the heat transmission and efficiency of a parabolic solar collector improved when the absorber tube was equipped with a torsional turbulator with rhombus-shaped cuts. Two models are presented: the first has one turbulator (N=1), while the second incorporates two turbulators (N=2). The turbulator thickness in these simulations is 1 mm, and the torsion ratio is established at 3. The incorporation of 5% concentrations of NanoAl2O3 and NanoCuO enhanced the thermal transfer between the base fluid (water) and the nanoparticles of both materials. Figure 1 depicts parabolic collector, absorber tube, and cross-sectional view with 6-torsion turbulator. The geometric features are shown in Table 1. The features of the nanofluid are delineated in Table 2.

Table 1
The magnitudes of the utilized parameters in the present study

Parameter	Re number (re)	Torsional ratio	Tube inner diameter (d)	Torsion length (y)	Turbulator width (w)	Turbulator length (l) (mm)	Turbulator thickness (t)	Cut length (l)	Cut width (w)
The magnitudes	20000 60000 100000	3	28	75	25	600	1	60	25

Table 2
The thermophysical features of nanoparticles and water [22]

	Cp (J/kgK)	ρ (kg/m^3)	k (W/mK)	μ (kg/ms)
Water	4181.8	998.2	0.6	0.001003
Al_2O_3	765	3900	30	-
CuO	531.8	6320	76.5	-

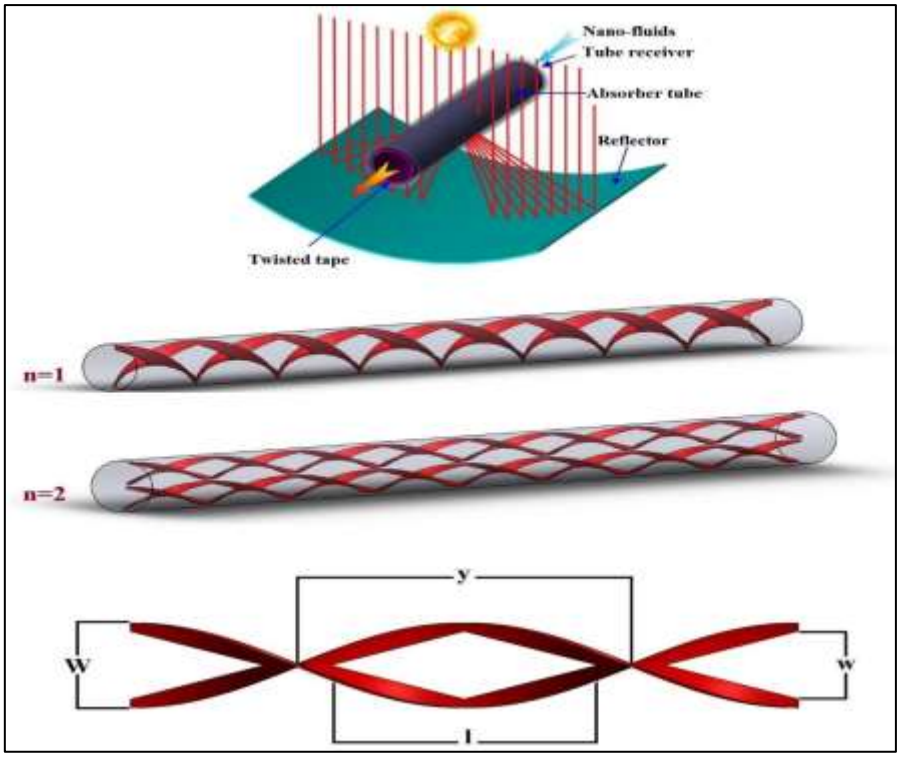

Fig. 1. The absorber tube is equipped with a torsional turbulator with rhombus-shaped cutting

3. Computational and Numerical Methods

3.1 The governing Equations

To simplify, it shall assume a constant flow rate, that the fluid was Newtonian and incompressible, and that gravitational effects are negligible. The governing formulas, which include energy, momentum, and continuity formulas, are delineated as follows depending on the fundamental presumptions and governing conditions [22,23]:

$$\frac{\partial \rho u_i}{\partial x_i} = 0 \tag{1}$$

$$\frac{\partial \rho u_i u_i}{\partial x_j} = \frac{\partial}{\partial x_j}\left[\mu\left(\frac{\partial u_i}{\partial x_j} + \frac{\partial u_i}{\partial x_i}\right) - \rho u_i \overline{u_j'}\right] - \frac{\partial p}{\partial x_i} \tag{2}$$

$$\frac{\partial \rho u_i T}{\partial x_j} = \frac{\partial}{\partial x_i}\left(\Gamma + \Gamma_t \frac{\partial T}{\partial x_i}\right) \tag{3}$$

where u_i denotes the component velocities, ρ is the density and μ is the dynamic viscosity, respectively. The k-Omega SST model is utilized to analyze turbulent flow, yielding the following relationships [24,25]:

$$\frac{\partial \rho k}{\partial_t} + \frac{\partial \rho k u_i}{\partial x_i} = \frac{\partial}{\partial x_j}\left(\Gamma_k \frac{\partial k}{\partial x_j}\right) + G_k - Y_k + S_k \tag{4}$$

$$\frac{\partial \rho \omega}{\partial t} + \frac{\partial \rho \omega_{u_j}}{\partial x_j} = \frac{\partial}{\partial x_i}\left(\Gamma_\omega \frac{\partial \omega}{\partial x_i}\right) + G_\omega - Y_\omega + D_\omega + S_\omega \tag{5}$$

The dynamics of a nanofluid including NanoCuO and NanoAl2O3 at a volume fraction of ϕ = 5% were analyzed using an effective single-phase model. The variables of this model may be delineated as follows [24]:

$$\rho_{\mathrm{eff}} = 1 - \varphi\rho_{\mathrm{f}} + \varphi\rho_{\mathrm{p}} \tag{6}$$

$$\mathrm{C}_{\mathrm{eff}} = \frac{1-\varphi\rho_{\mathrm{f}}\mathrm{C}_{\mathrm{f}}+\varphi\rho_{\mathrm{P}}\mathrm{C}_{\mathrm{P}}}{\rho_{\mathrm{eff}}} \tag{7}$$

$$\mu_{\mathrm{sff}} = \frac{\mu_{\mathrm{f}}}{1-\varphi^{2.5}} \tag{8}$$

$$\frac{\mathrm{k}_{\mathrm{eff}}}{\mathrm{k}_{\mathrm{f}}} = \frac{\mathrm{k}_{\mathrm{p}}+2\mathrm{k}_{\mathrm{f}}+2\varphi\mathrm{k}_{\mathrm{P}}-\mathrm{k}_{\mathrm{f}}}{\mathrm{k}_{\mathrm{P}}+2\mathrm{k}_{\mathrm{f}}-2\varphi\mathrm{k}_{\mathrm{P}}-\mathrm{k}_{\mathrm{f}}} \tag{9}$$

where ρ_{eff}, is the effective density, C_{eff} is the effective specific heat, k_{eff} is the effective viscosity, and k_{eff} is the effective thermal conductivity. nano is the nanoparticle volume fraction, f is the fluid, and p is the particle. Analyses of heat transmission were simulated using parameters including collector efficiencies, performance evaluation criteria (PEC) , factor of frictions (f), Nu and, dimensionless Re [22,23,26].

$$\mathrm{Re} = \frac{\rho\mathrm{uD}}{\mu} \tag{10}$$

$$Nu_{avg} = \frac{hD}{k} \tag{11}$$

The following formula determines the factor of friction:

$$f = \frac{2\Delta PD}{\rho\mathrm{Lu}^2} \tag{12}$$

Within a heat exchanger or solar receiver, the PEC evaluates the thermal features of the fluid flow. Under constant friction, this coefficient can be described as the proportion of the displacement heat transfer rate (Nu/Nup) to the factor of friction (f/fp) [27].

$$\mathrm{PEC} = \frac{\mathrm{Nu}/\mathrm{Nu}_{\mathrm{P}}}{\mathrm{f}/\mathrm{f}_{\mathrm{P}}^{1/3}} \tag{13}$$

In this context, Nu and Nup represent the Nu for the tube and the tube equipped with a twisted tape cut in a circular configuration, respectively. In this context, fp represents the factor of friction of the tube, while f denotes the factor of friction of the tube in conjunction with the equipment. Both fp and f are calculated by utilizing a twisted tape that has been fashioned into a circular form. The thermal efficiency of solar collectors is assessed to gauge their thermal performance. Thermal efficiency may be calculated by dividing the energy reflected by a reflecting plate's surface by the energy absorbed by the fluid in the absorber tube.

$$\eta_c = \frac{\dot{m}_{in}\mathrm{T}_{\mathrm{out}}-T_{in}}{6\times10^4 IA} \tag{14}$$

3.2 Boundary Conditions

Air enters the absorber tube with a uniform axial velocity and at a consistent temp. Defining the features and Re of the nanofluid utilized for velocity calculations. The outlet pressure is selected as the ultimate working state, as seen in Figure 2. This is achieved by supplying a steady heat flux to the absorber tube wall while preserving adiabatic boundaries along the turbulator wall (Table 3).

Table 3
The boundary conditions of the problem

Location	Boundary conditions
Inlet	Uniform velocity and temp ($u=u_0$ and $T=T_0=313.15$ K)
Tube wall	Uniform heat flux (30000 W/m^2)
Outlet	The condition of zero pressure gradient

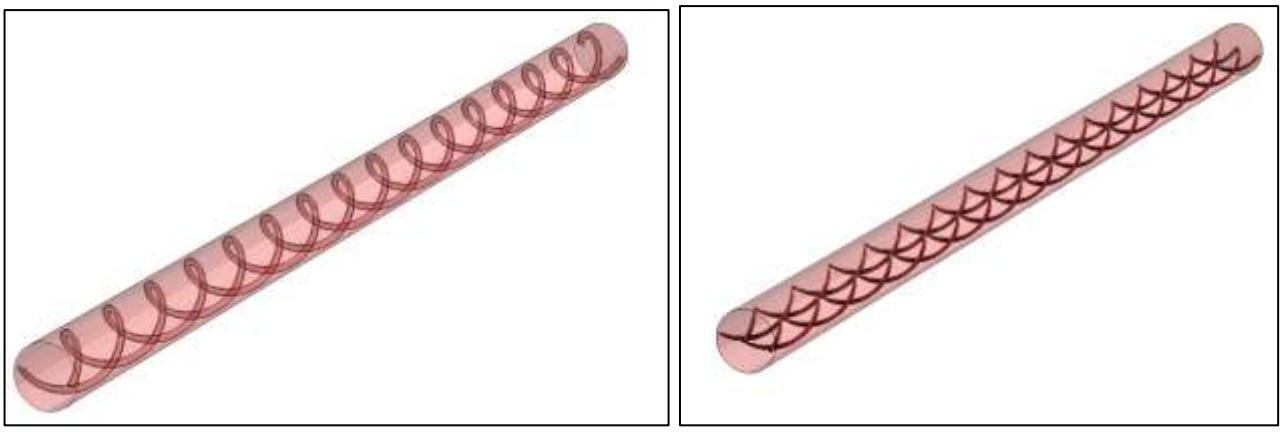

Fig. 2. The applied boundary conditions to the absorber tube with turbulator

3.3 Grid Independency

ANSYS Meshing 2020 is utilized to generate a mesh for the computational domain. Given that most the fluid's velocity variations transpire at the walls, a boundary layer mesh is utilized in that area, particularly next to the turbulator and the tube wall, as seen in Figure 3. The mesh may be adjusted in boundary layer areas to enhance precision near the geometry. The selected turbulence model maintains the wall's dimensionless distance, y+, hence enhancing accuracy. Consequently, we are discussing a reduced meshing element size next to the absorber tube wall and an increased size in other areas of the domain to accommodate the turbulator. Verifying the independence of results from the produced meshing is crucial for selecting the optimal meshing to provide accurate replies. Consequently, the Nu, a variable in the research, was computed across five separate meshes composed of various sorts of components. Table 4 indicates little fluctuation in the Nu within a range of 2,700,000 to 3,250,000 items. A main mesh with 2,700,000 components was utilized to expedite the computations.

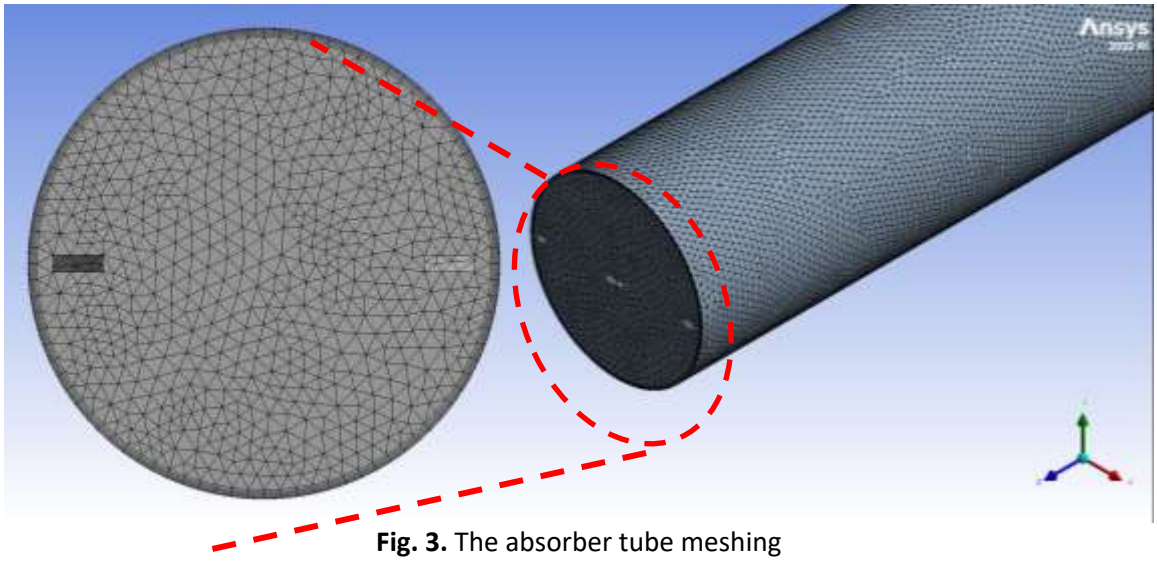

Fig. 3. The absorber tube meshing

Table 4
Grid independence results for Nu

Error percentage	Nu	Elements Number
-	828.2	1050000
6.3%	880.5	1620000
4.5%	919.8	2140000
3.5%	952.7	2750000
0.6%	959.2	3210000

3.4 Validation

The collecting findings using numerical approaches and juxtaposing them with credible numerical or laboratory data is crucial for validating the legitimacy of the simulation outcomes. To assess the accuracy of the present study. The factor of friction inside an adsorber tube, both without a turbulator and with NanoAl2O3, was first examined. Figure 4 illustrates the results across several Reynolds magnitudes. In accordance with the results [28], as seen in Figure 4, the friction coefficient of the simulated model in the current investigation resembles that observed in their research. Consequently, trust in the modeling outcomes may be affirmed.

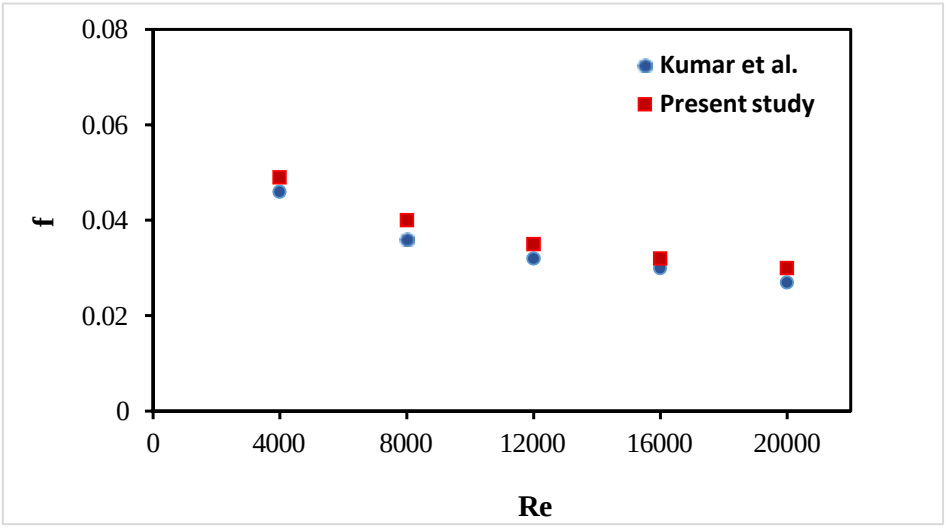

Fig. 4. Factor of friction per Re in this study [28]

4. Results And Discussion

This section reviews and discusses results from numerical simulations of a parabolic collector's absorber tube, featuring a rhombic-shaped turbulator and nanoparticles. Two models are examined: the first with N=1 and the second with N=2. The parameters assessed include collector efficiency, PEC, factor of friction (f), Nu, the coefficient of Convective heating transfer (h), and pressure drops (P) at Re of 100000, 60000, and 20000 to determine the optimal shape. The temp distribution at the absorber tube's exit is illustrated in Figures 5 and 6. Figure 5 shows the temp distribution at the absorber tube outlet for two water conditions (N=1 and N=2) without nanoparticles is evaluated across Re (Re = 20000, 60000, and 100000). At Re = 20000, both water conditions exhibit significant temp gradients, with elevated temps near the walls and cooler regions towards the center. As the Re increases, the temp distribution becomes increasingly uniform. At Re = 60000, and particularly at Re = 100000, the temp field is dominated by cooler zones, indicating enhanced convective heat transfer and thermal homogeneity. This trend is consistent for both water conditions, showcasing reduced temp disparities at higher Re.

In accordance with the boundary conditions of the issue, the output temp increases due to the absorber tube getting a uniform heat flow. The outlet temp and Re exhibit an inverse relationship, with the outlet temp reducing as the Re increases.

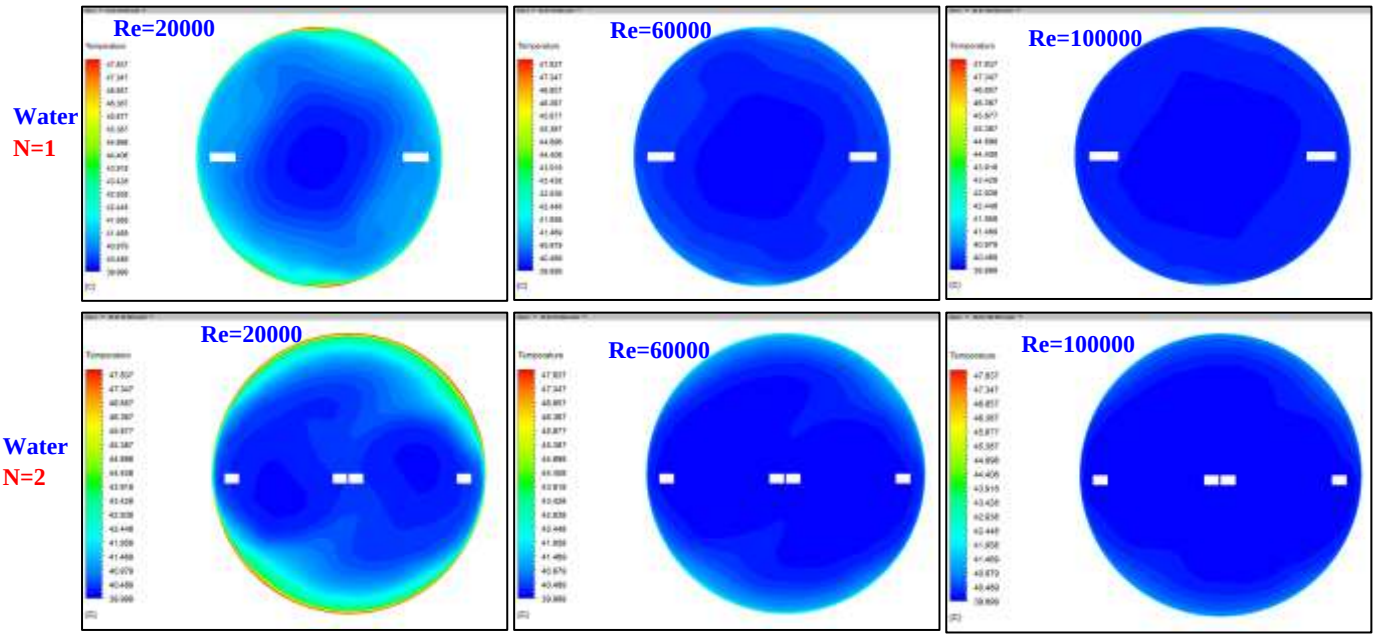

Fig. 5. Temp distribution in the absorber tube outlet in various models with water fluid

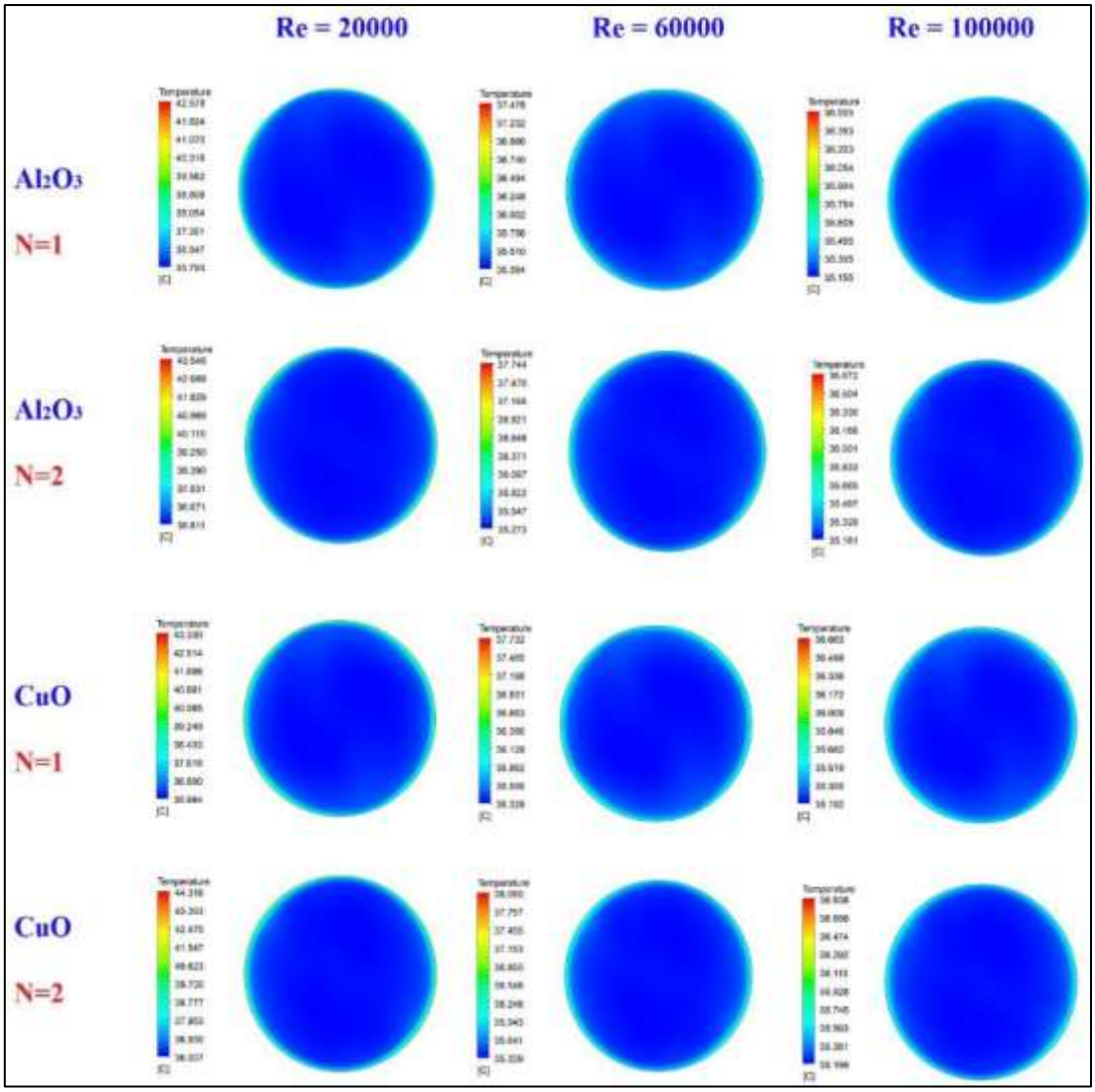

Fig. 6. Temp distribution in the absorber tube outlet in various models with water and various nano Al2O3 and CuO

The temp distribution along the absorber tube equipped with one and N=2 at Re = 20000, in the absence of nanoparticles shown in Figure 7, demonstrates distinct thermal features. In the case of (N=1), a helical temp pattern is observed, with alternating high and low-temp zones due to localized enhancement of heat transfer, reaching a maximum of 53.612°C. Conversely, with N=2, the distribution is more uniform, exhibiting reduced periodicity and smoother transitions between thermal zones, leading to improved overall thermal homogeneity. The additional turbulator enhances the mixing and heat transfer, minimizing temp disparities along the tube's length.

The fluid outlet temp is more profoundly influenced by CuO nanoparticle-infused nanofluids than by Al2O3-infused nanofluids. The output temp is elevated in models using two torsional turbulators (N=2) compared to those with a single turbocharger (N=1) because of the increased effective heat level. The peak output temp, around 46 degrees centigrade, has risen by 31% relative to the fluid input temp of 35degree centigrade, occurring next to the adsorber tube with two tabulators with NanoCuO at Re=20000. The temp distribution for this representation along the tube that absorbs heat is seen in Figure 8.

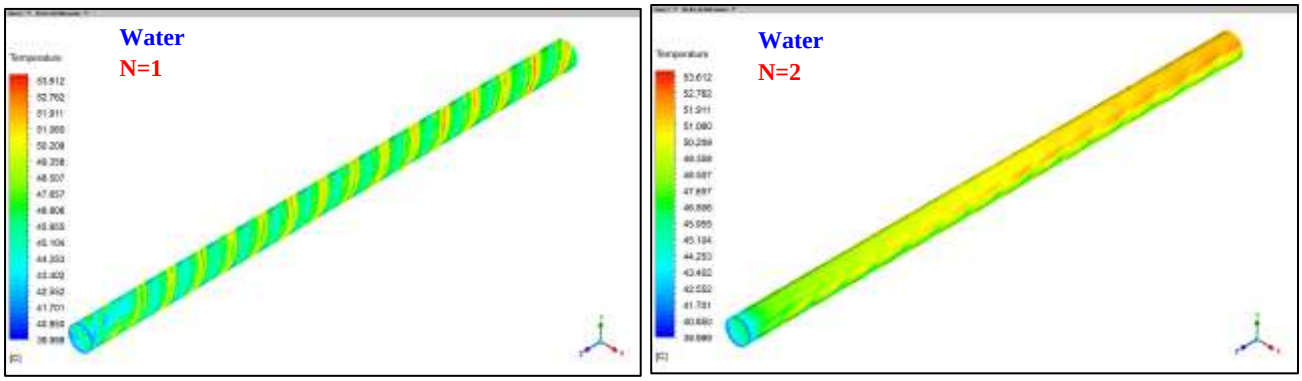

Fig. 7. Temp distribution in the adsorber tube in N=1 and N=2 without nanoparticles and Re=20000

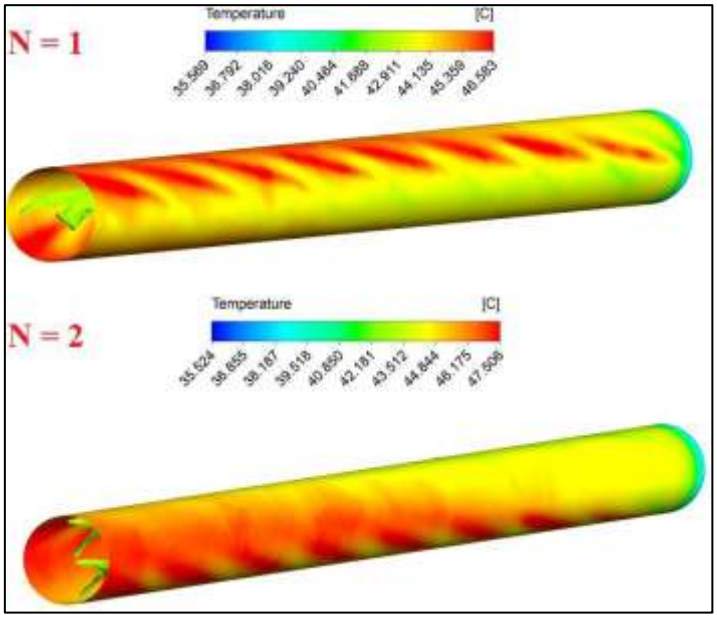

Fig. 8. Temp distribution in the adsorber tube in N=1 and N=2 in the existence of NanoCuO and Re=20000

Figure 9 shows the pressure in the tube when applying water without any nanoparticle's additives, the pressure was decreased significantly when (N=2) comparison with (N=1) for all selected Re. At higher Re, the velocity escalates, resulting in a maximum pressure loss at Re=100000. The existence of NanoAl2O3 and NanoCuO at Re=100000 induces a pressure change along the absorber tube fitted with a torsional turbulator, as seen in Figure 10 for two models (N =1, 2). Conversely, the fluid pressure progressively decreases as it nears the outflow. Ultimately, the boundary conditions of the issue stipulate that the pressure at the outflow is equivalent to atmospheric pressure (zero relative pressure). N=1 model has a higher pressure drop than two turbulator models. Models using CuO fluid exhibit a more significant pressure reduction due to the higher density of NanoCuO compared to those of Al2O3.

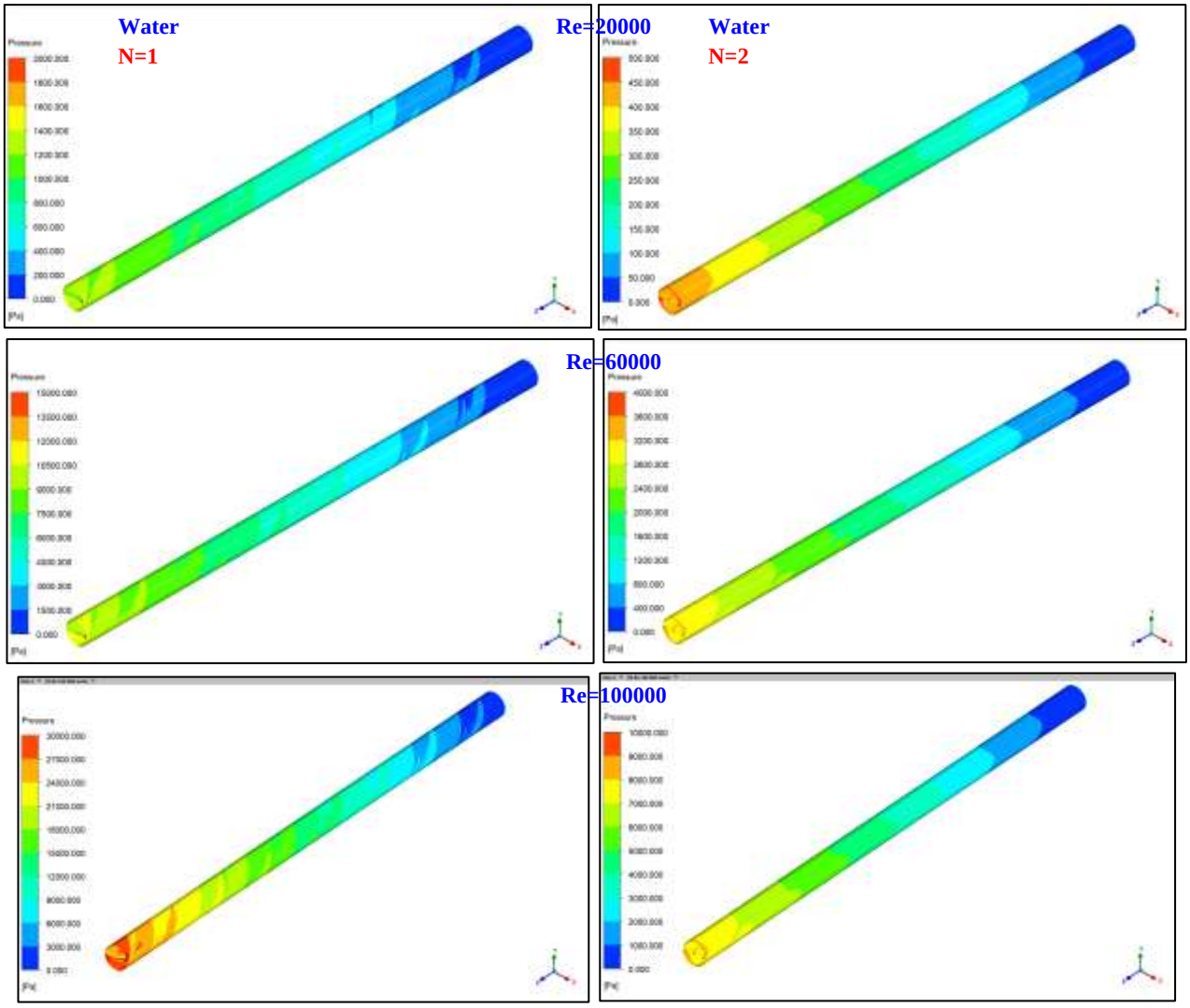

Fig. 9. Pressure variation based on Re magnitude for N=1 and N=2 in water without nanoparticles

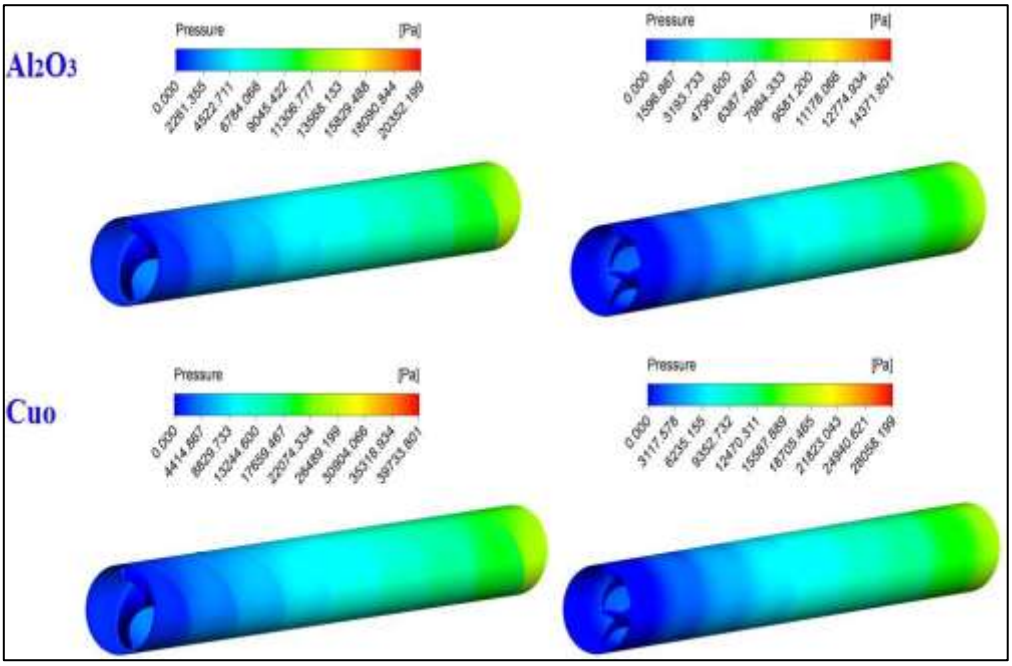

Fig. 10. Pressure drops in Re= 100000 in four various models

Figure 11, the velocity distribution and streamline behavior in the absorber tube at Re of 20000, 60000, and 100000, without additives, demonstrate distinct flow features for both Water N=1 and Water N=2. At Re = 20000, Water N=1 shows lower velocities (up to 0.98 m/s) with strong helical vortices, while Water N=2 exhibits smoother, more streamlined flow. As the Re increases to 60000 and 100000, peak velocities reach 3.0 m/s and 5.0 m/s, respectively, with both configurations experiencing enhanced turbulence. However, Water N=2 maintains more organized flow, whereas Water N=1 demonstrates more chaotic vortex structures, indicating stronger localized mixing near the turbulators.

Figure 12 illustrates the velocity distribution along the absorber tube for various types via streamlines. At increased Re, the flow velocity increases. N=1 model has greater velocities than two turbulator models. The flow rate of models with NanoCuO exceeds that of models with NanoAl2O3.

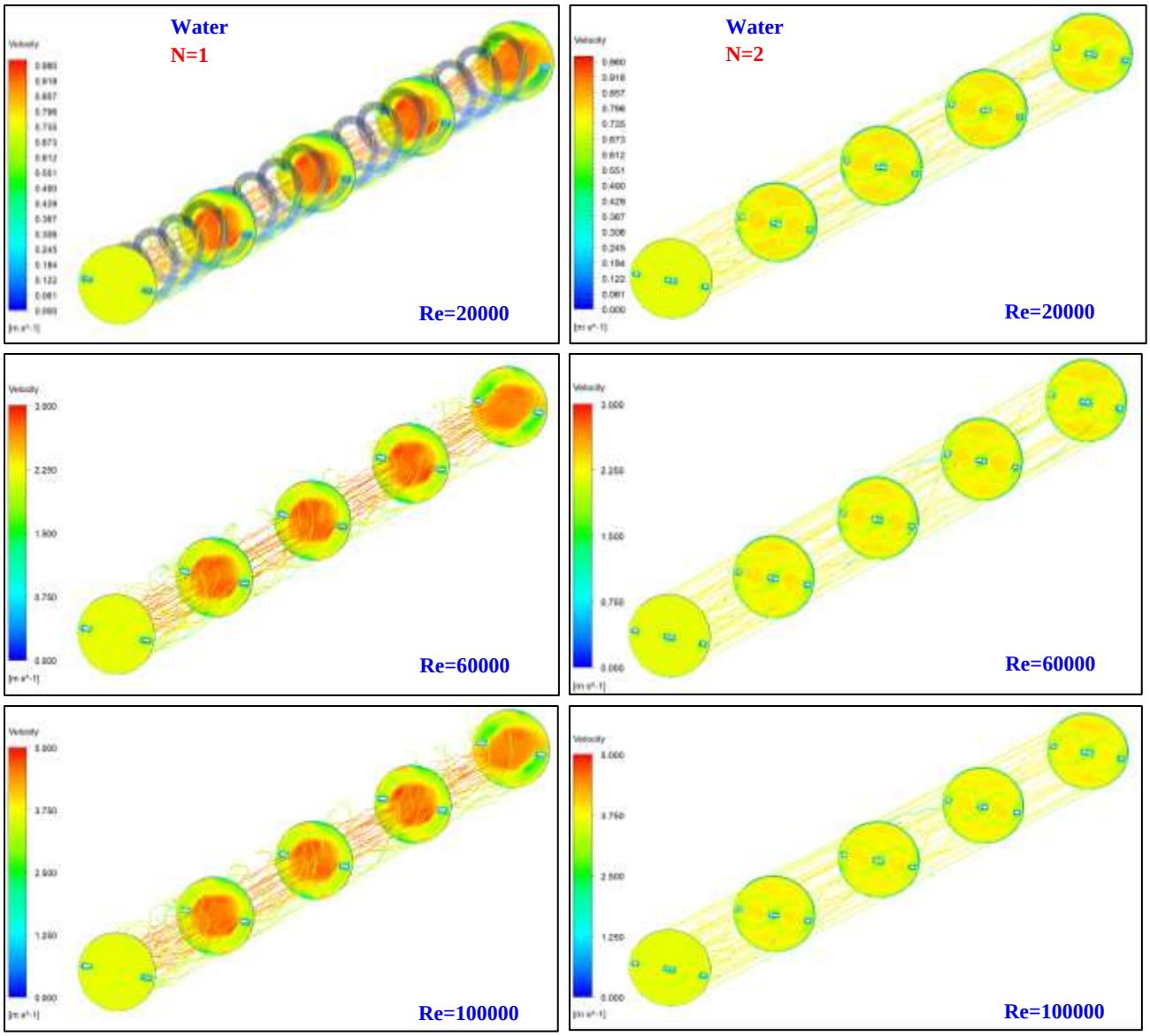

Fig. 11. Velocity distribution and streamlines in various Re under the absence of nanoparticles

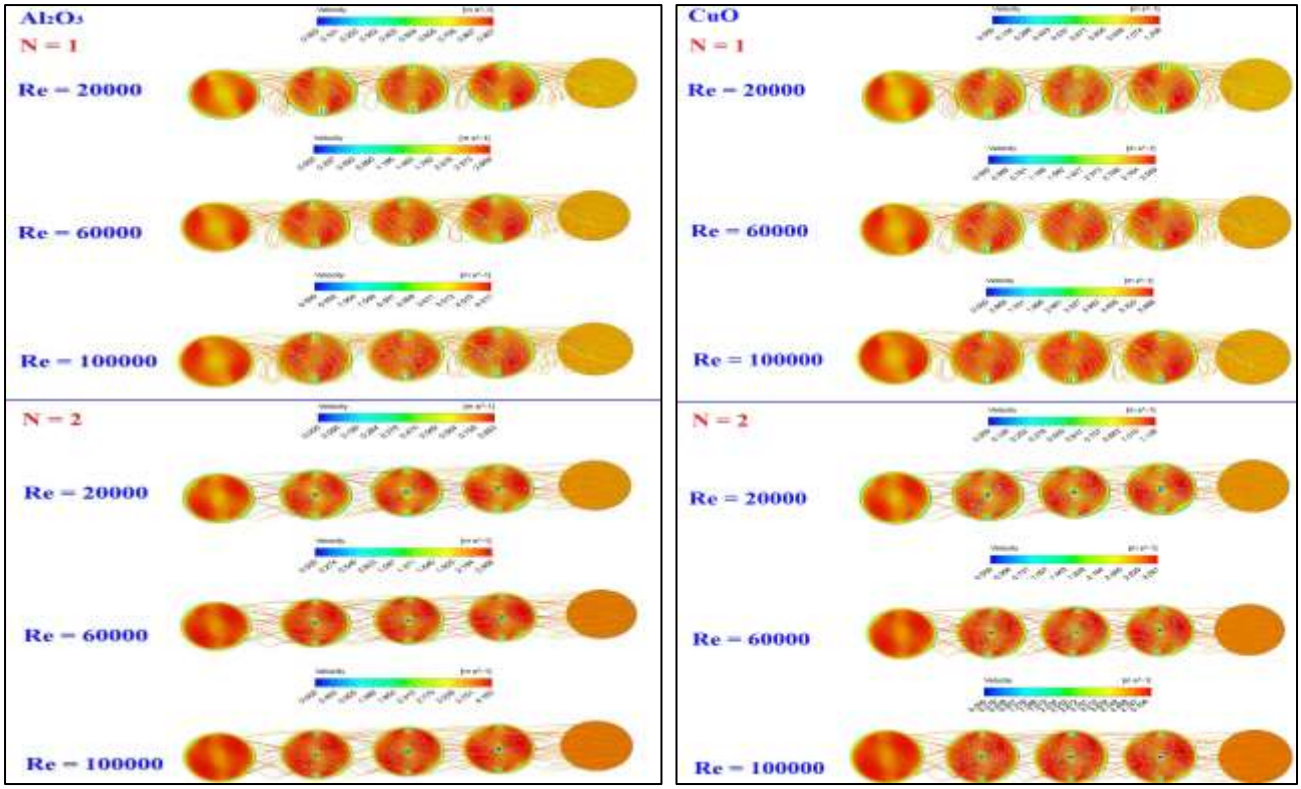

Fig. 12. Velocity distribution and streamlines in various Re under the existence of NanoAl2O3 and NanoCuO

Figure 13 illustrates the variation of pressure drop (ΔP) with Re for two water models (N=1 and N=2) in the absence of nanoparticles. As Re increases, a pronounced rise in pressure drop is observed for both models, with Water N=1 exhibiting significantly higher-pressure losses compared to Water N=2. At low Re (Re = 20000), both models show minimal pressure drop; however, as Re reaches 60000 and 100000, Water N=1 demonstrates a steep increase, peaking near 30,000 Pa. In contrast, Water N=2 experiences a more gradual rise, reaching just over 10,000 Pa, indicating enhanced flow resistance and turbulence in Water N=1.

Figure 14 illustrates the pressure progression inside an adsorber tube fitted with a rhombic-shaped torsional turbulator, including NanoAl2O3 and NanoCuO at Re of 20000, 60000, and 100000. The incorporation of nanoparticles into a base fluid increases the viscosity of the fluid. This action results in a more significant reduction in pressure compared to a base fluid (water). Comparing the pressure decreases induced by NanoAl2O3 and NanoCuO reveals that the former has a more significant impact. A high Re correlates with a substantial pressure decrease. An examination of Figure 9 indicates that the model with N=1 exhibits a greater pressure drop compared to the model with N=2. In other terms, at Re=100000, the pressure drops for N=1 NanoCuO is 24736.6 Pa, but at Re=20000, the pressure drop for NanoAl2O3 is just 706.4 Pa (according to the utilized model).

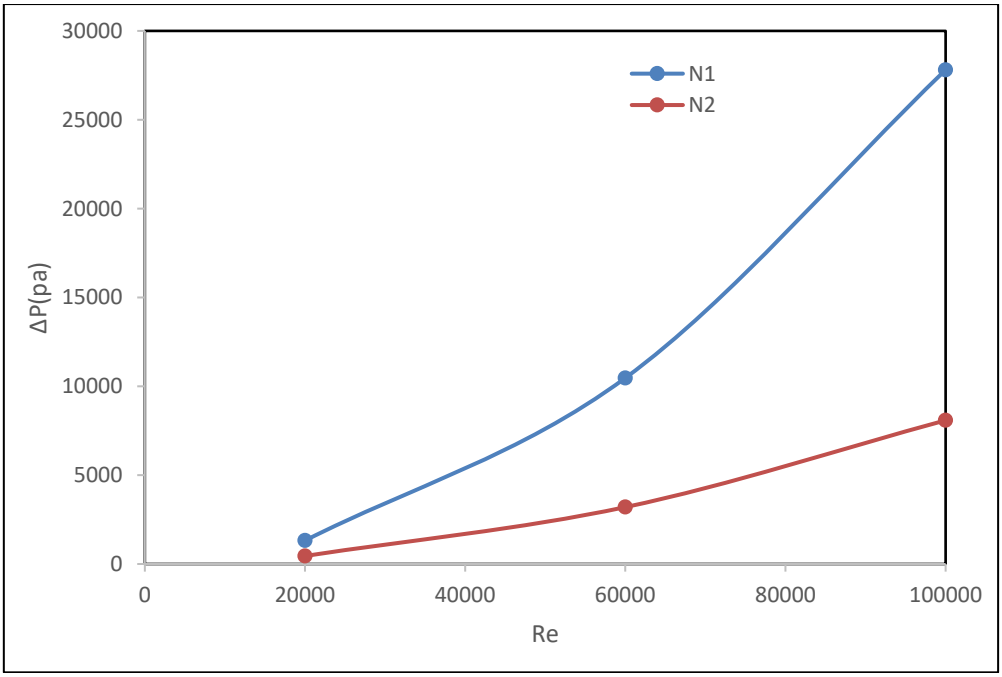

Fig. 13. Pressure drops against Re in for water models without nanoparticles

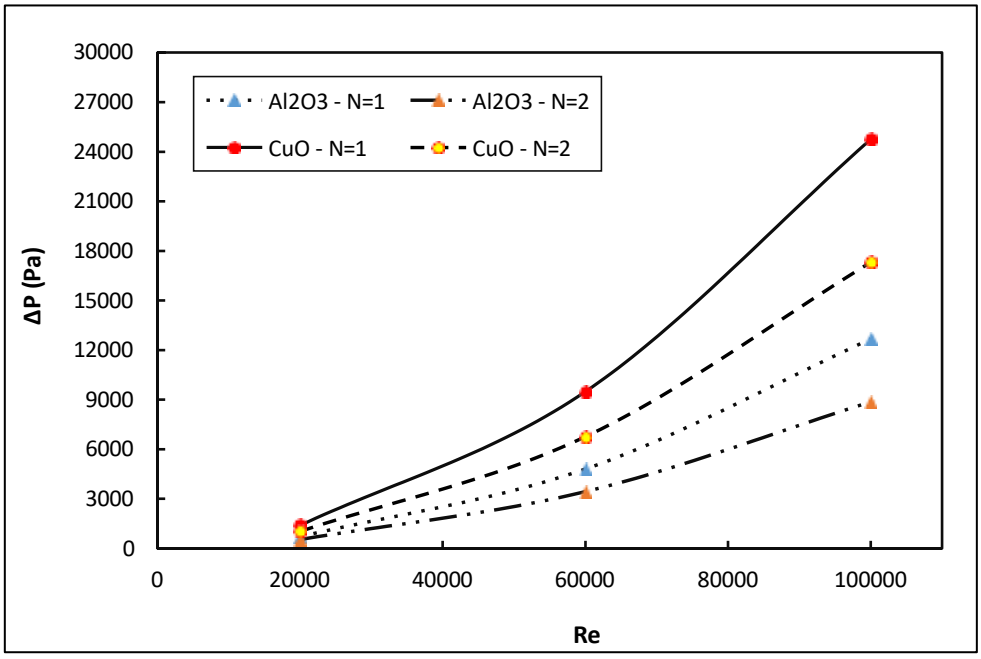

Fig. 14. Pressure drops against Re in various models

Figure 15 displays the relationship between the the coefficient of convective heating transfer (h) and Re for two water models, $\mathrm{N} = 1$ and $\mathrm{N} = 2$, without nanoparticles. Both curves demonstrate an increase in the heat transfer coefficient as the Re rises from 20000 to around 100000. Specifically, Water $\mathrm{N} = 1$ starts at approximately $950\frac{\mathrm{W}}{\mathrm{m}^2 K}$ and ascends to about $1130\frac{\mathrm{W}}{\mathrm{m}^2\,\mathrm{K}}$, showing a stronger increase compared to Water $\mathrm{N} = 2$, which begins around $900\frac{\mathrm{W}}{\mathrm{m}^2 K}$ and increases to just below $1100\frac{W}{m^2 K}$. The trend indicates that as flow velocity increases (reflected by a higher Re), the ability of the water to convectively transfer heat improves, likely due to enhanced turbulence and more effective mixing of the fluid layers near the heat transfer surfaces.

A variety of models' the coefficient of convective heating transfers is depicted in Figure 16. When comparing models with and without Al2O3, models with NanoCuO have a higher coefficient of Convective heating transfer. However, in models with a single turbulator, this coefficient is significantly bigger than in those with two.

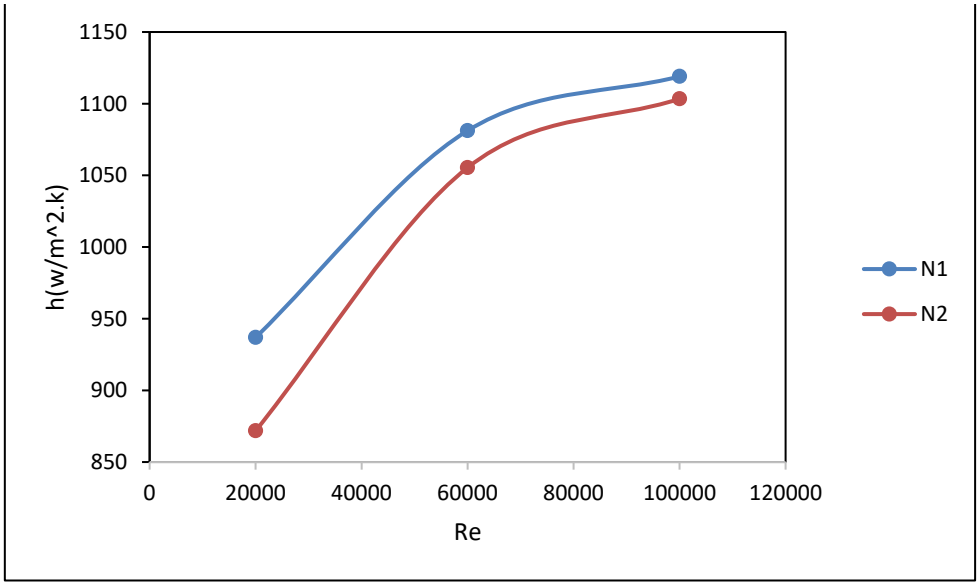

Fig. 15. The coefficient of convective heating transfer against Re for water models without nanoparticles

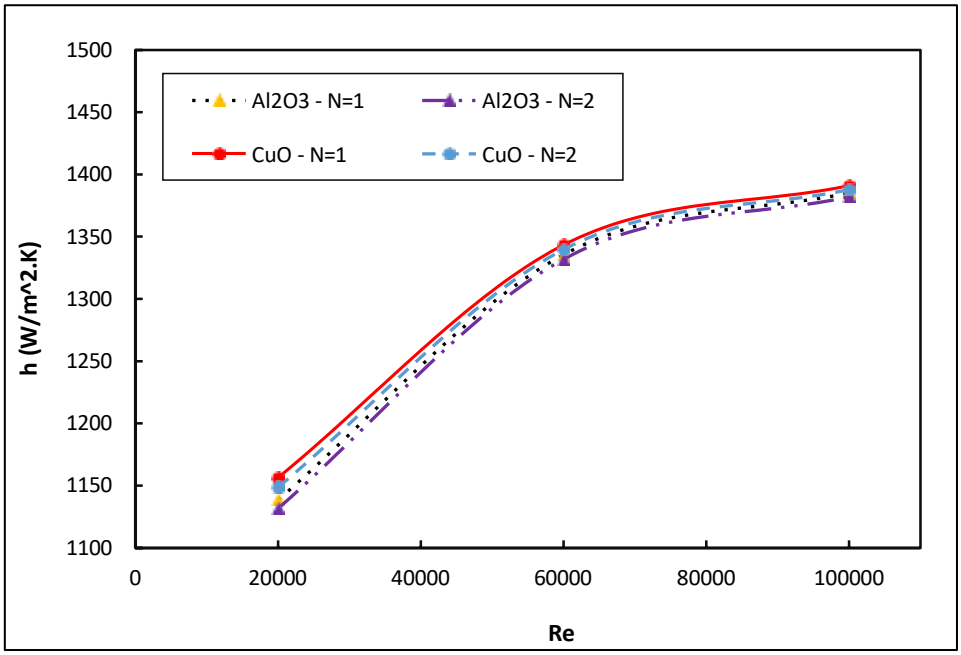

Fig. 16. The coefficient of convective heating transfer against Re for water models with various nanoparticles

Figure 17 presents the relationship between the Nu and Re for two water models, N=1 and N=2, without nanoparticles. Both models demonstrate an upward trend in Nu with increasing Re, reflecting improved convective heat transfer as flow velocity rises. Water N=1 consistently achieves higher Nu compared to Water N=2, indicating superior heat transfer performance. Specifically, Water N=1 sees an increase from approximately 1550 at Re = 20000 to around 1875 at Re = 100000, while

Water N=2 rises from 1450 to 1800. The results suggest that Water N=1 benefits from enhanced turbulence, leading to more efficient thermal energy transfer.

Figure 18 illustrates the Nu outcomes with NanoAl2O3 and NanoCuO at Re of 20000, 60000, and 100000 for the adsorber tube fitted with a torsional turbulator in two distinct models (N=1, 2). In all models, it is evident that an increase in the Re corresponds with an increase in the Nu. The Nu for models including CuO nanoparticles exceeds that of models with NanoAl2O3 due to the distinct physical features of CuO nanoparticles. The Nu is closely related to the the coefficient of Convective heating transfer; hence, the variations in Nusselt diagrams across various models mirror the trends seen in the diagrams of the the coefficient of Convective heating transfer. At Re=100000, the models using NanoCuO exhibited a Nu of around 1230, the highest recorded. For Re=20000, the models including NanoAl2O3 have the lowest Nu, about 950.

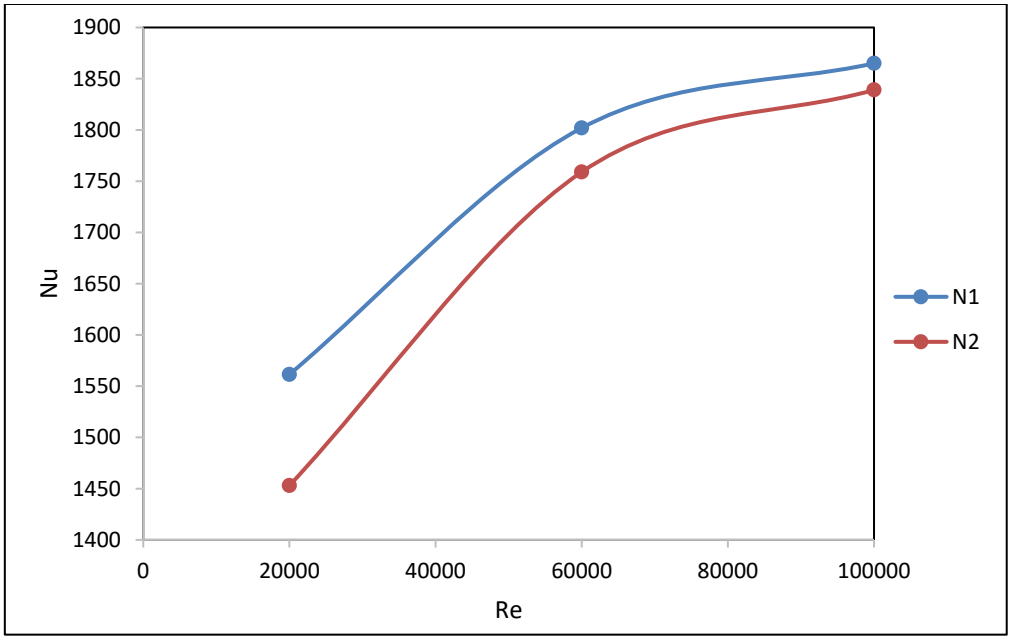

Fig. 17. Nu against Re for various models

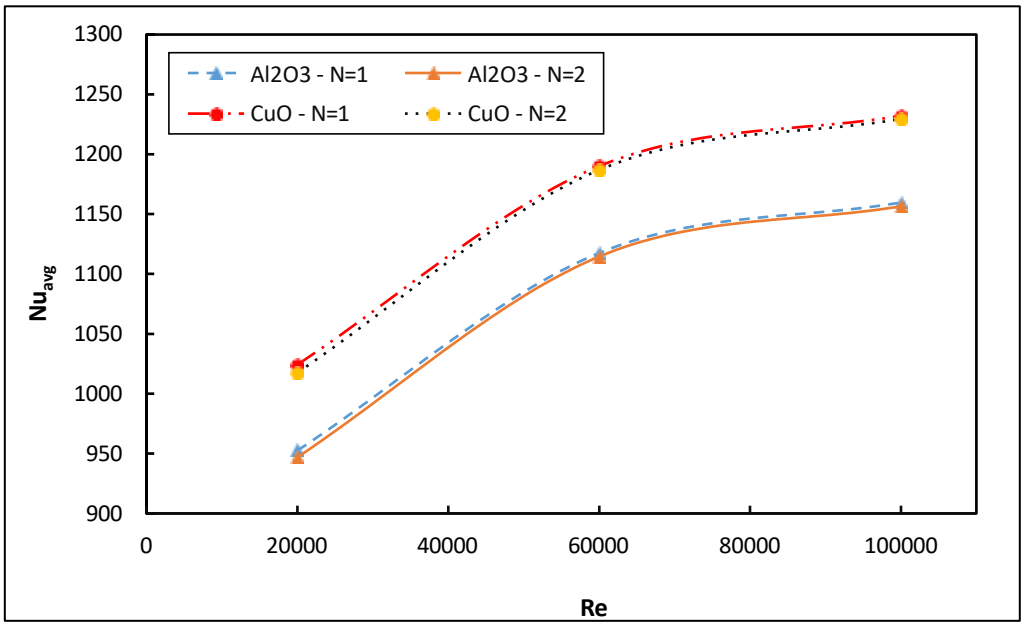

Fig. 18. Nu against Re for various models

Figure 19 illustrates the relationship between the factor of friction (f) and Re for two water models, N=1 and N=2, without nanoparticles. Both models exhibit a decreasing trend in the factor of friction as the Re increases, indicating reduced frictional resistance with higher flow velocities. Water N=1 consistently demonstrates a higher factor of friction than Water N=2, suggesting greater turbulence or surface interaction. Specifically, Water N=1 decreases from approximately 0.21 at Re = 20000 to 0.16 at Re = 100000, while Water N=2 drops from around 0.08 to 0.05. This highlights that Water N=1 experiences higher frictional losses compared to Water N=2.

Figure 20 presents a comparison of the factor of friction across several models. Increasing the Re may elevate both the velocity and the pressure decrease. According to the equation, these two components affect the friction coefficient (12). A reduction in pressure is directly proportional to the factor of friction, which is inversely proportional to the square of the velocity. As the Re escalates, the fluid velocity significantly rises, diminishing the factor of friction despite the augmented pressure drop. The factor of friction is 34% greater in N=1 turbulator mode compared to N=2 turbulator mode. At a Re of 20000, the adsorber tube fitted with a turbulator exhibits a peak factor of friction of 0.117 attributable to the existence of NanoCuO. When N=2 is included into an adsorber tube filled with a fluid with NanoAl2O3, the pressure loss remains negligible at a Re of 100000. The factor of friction in this circumstance is 0.055.

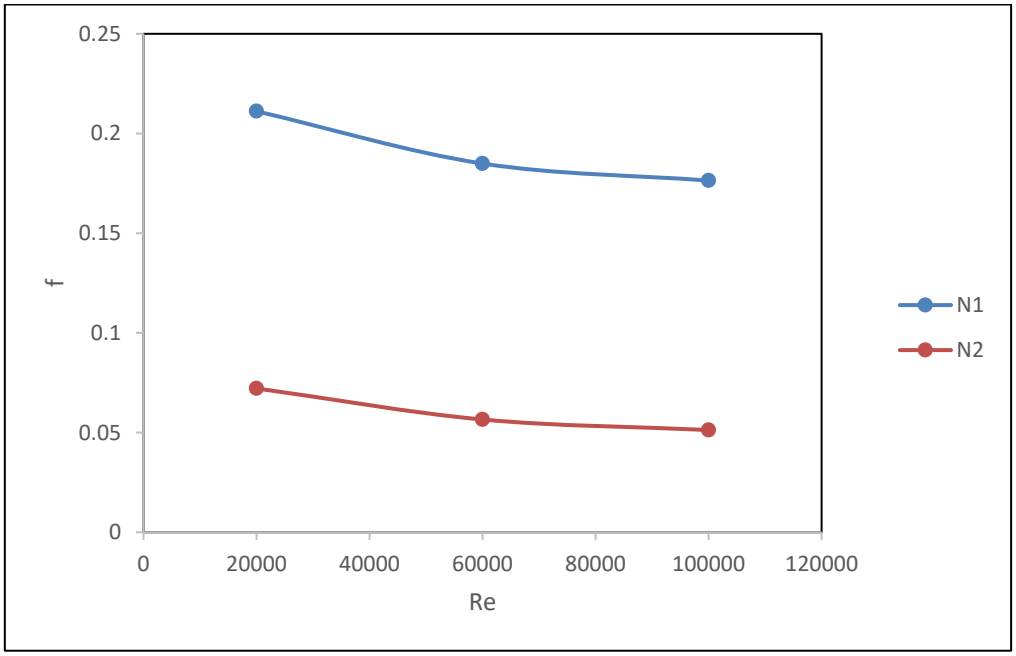

Fig. 19. The factor of friction against Re for water models without nanoparticles

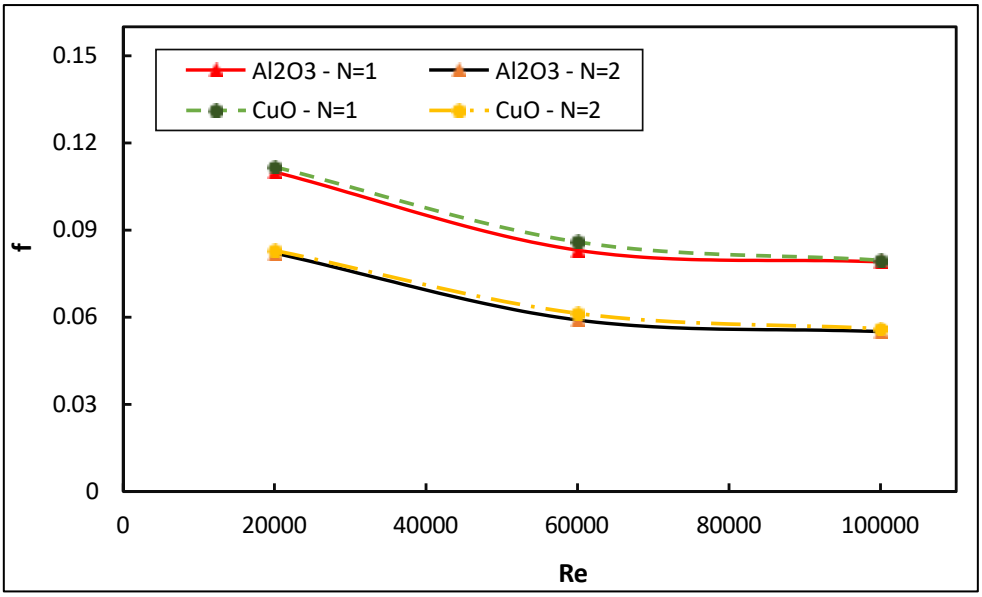

Fig. 20. The factor of friction against Re for various models

Upon analyzing the Eq. (13), it is evident that the PEC is directly proportional to the Nu and inversely proportional to the factor of friction. The Nu and the factor of friction both enhanced with an increase in the Re. Thus, as seen in Figure 21, an increase in the Re corresponds with a rise in the PEC. Dual-tubular models surpass single-turbulator ones regarding PEC. The PEC of N=2 models is about 12% more than that of N=1 model throughout a broad spectrum of Reynolds magnitudes. In comparison to NanoAl2O3, NanoCuO have a more pronounced effect on heat conductivity. The PEC reaches its maximum magnitude of 1.39 at Re=100000 while utilizing NanoCuO in a two-turbulator model.

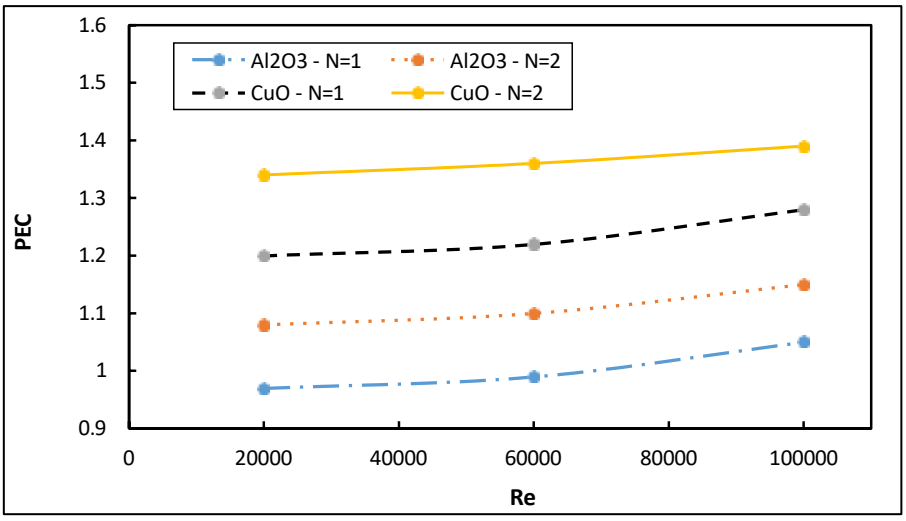

Fig. 21. PEC against Re for various models

The thermal efficiency of solar collectors is a crucial parameter for assessing collector performance. Figure 22 illustrates the variation of this parameter with the Re for two unique models (N=1, 2) of a solar collector, utilizing NanoAl2O3 and NanoCuO, which is equipped with an adsorber tube including a torsional turbulator with rhombic-shaped cuts. Research indicates that the nanofluid receiver exhibits enhanced solar energy absorption when NanoCuO is utilized in place of Al2O3. Thus,

the two variants of turbulators containing NanoCuO produce the most thermal energy under the ideal working state of Re=100000.

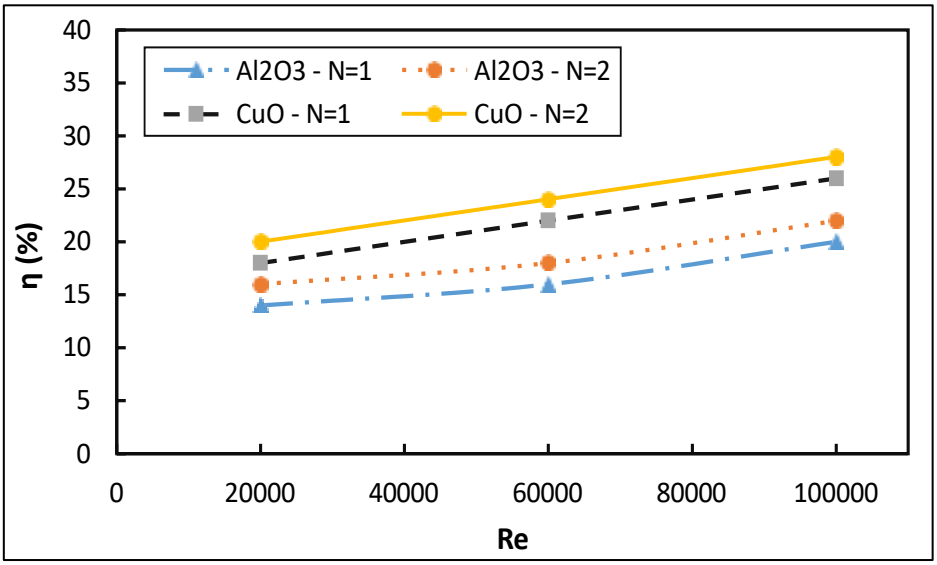

Fig. 22. Solar collector efficiency per Re in various models

5. Conclusion

The figure presents the relationship between the factor of friction (f) and Re for two water models, N=1 and N=2, in the absence of nanoparticles. Both models exhibit a declining factor of friction with increasing Re, indicating a reduction in frictional losses as flow velocity increases. Water N=1 consistently shows a higher factor of friction across all Re, suggesting increased turbulence or surface interaction compared to Water N=2. Specifically, Water N=1's factor of friction decreases from approximately 0.21 at Re = 20000 to 0.16 at Re = 100000, while Water N=2 reduces from 0.08 to 0.05 over the same range. This trend highlights that Water N=1 experiences more significant frictional resistance, which may be attributed to higher turbulence or the geometric effects of the turbulators. Consequently, although both models demonstrate reduced friction with higher Re, Water N=2 offers more efficient flow with lower frictional losses, making it potentially more favorable for applications where minimizing energy losses is critical.

References

[1] Wijayanta, Agung Tri, Tri Istanto, Keishi Kariya, and Akio Miyara. "Heat transfer enhancement of internal flow by inserting punched delta winglet vortex generators with various attack angles." *Experimental Thermal and Fluid Science* 87 (2017): 141-148. https://doi.org/10.1016/j.expthermflusci.2017.05.002

[2] Yaningsih, Indri, Tri Istanto, and Agung Tri Wijayanta. "Experimental study of heat transfer enhancement in a concentric double pipe heat exchanger with different axial pitch ratio of perforated twisted tape inserts." In *AIP Conference Proceedings*, vol. 1717, no. 1. AIP Publishing, 2016. https://doi.org/10.1063/1.4943436

[3] Mohammed, H. A., Husam A. Hasan, and M. A. Wahid. "Heat transfer enhancement of nanofluids in a double pipe heat exchanger with louvered strip inserts." *International Communications in Heat and Mass Transfer* 40 (2013): 36-46. https://doi.org/10.1016/j.icheatmasstransfer.2012.10.023

[4] Chougule, Sandesh S., and S. K. Sahu. "Heat transfer and friction characteristics of Al2O3/water and CNT/water nanofluids in transition flow using helical screw tape inserts–a comparative study." *Chemical Engineering and Processing: Process Intensification* 88 (2015): 78-88. https://doi.org/10.1016/j.cep.2014.12.005

[5] Yakut, Kenan, and Bayram Sahin. "The effects of vortex characteristics on performance of coiled wire turbulators used for heat transfer augmentation." *Applied Thermal Engineering* 24, no. 16 (2004): 2427-2438. https://doi.org/10.1016/j.applthermaleng.2004.03.008

[6] Naphon, Paisarn. "Experimental investigation the nanofluids heat transfer characteristics in horizontal spirally coiled tubes." *International Journal of Heat and Mass Transfer* 93 (2016): 293-300. https://doi.org/10.1016/j.ijheatmasstransfer.2015.09.089

[7] Naphon, P., S. Wiriyasart, T. Arisariyawong, and T. Nualboonrueng. "Magnetic field effect on the nanofluids convective heat transfer and pressure drop in the spirally coiled tubes." *International journal of heat and mass transfer* 110 (2017): 739-745. https://doi.org/10.1016/j.ijheatmasstransfer.2017.03.077

[8] Narrein, K., and H. A. Mohammed. "Influence of nanofluids and rotation on helically coiled tube heat exchanger performance." *Thermochimica Acta* 564 (2013): 13-23. https://doi.org/10.1016/j.tca.2013.04.004

[9] Kannadasan, N., K. Ramanathan, and S. Suresh. "Comparison of heat transfer and pressure drop in horizontal and vertical helically coiled heat exchanger with CuO/water based nano fluids." *Experimental Thermal and Fluid Science* 42 (2012): 64-70. https://doi.org/10.1016/j.expthermflusci.2012.03.031

[10] Mohammed, Hussein A., and K. Narrein. "Thermal and hydraulic characteristics of nanofluid flow in a helically coiled tube heat exchanger." *International Communications in Heat and Mass Transfer* 39, no. 9 (2012): 1375-1383. https://doi.org/10.1016/j.icheatmasstransfer.2012.07.019

[11] Hashemi, S. M., and M. A. Akhavan-Behabadi. "An empirical study on heat transfer and pressure drop characteristics of CuO–base oil nanofluid flow in a horizontal helically coiled tube under constant heat flux." *International Communications in Heat and Mass Transfer* 39, no. 1 (2012): 144-151. https://doi.org/10.1016/j.icheatmasstransfer.2011.09.002

[12] Akhavan-Behabadi, M. A., M. Fakoor Pakdaman, and M. Ghazvini. "Experimental investigation on the convective heat transfer of nanofluid flow inside vertical helically coiled tubes under uniform wall temperature condition." *International Communications in Heat and Mass Transfer* 39, no. 4 (2012): 556-564. https://doi.org/10.1016/j.icheatmasstransfer.2012.02.008

[13] Darzi, AA Rabienataj, Mousa Farhadi, Kurosh Sedighi, Shahriar Aallahyari, and Mojtaba Aghajani Delavar. "Turbulent heat transfer of Al2O3–water nanofluid inside helically corrugated tubes: numerical study." *International Communications in Heat and Mass Transfer* 41 (2013): 68-75. https://doi.org/10.1016/j.icheatmasstransfer.2012.11.006

[14] Jaisankar, S., T. K. Radhakrishnan, K. N. Sheeba, and S. Suresh. "Experimental investigation of heat transfer and friction factor characteristics of thermosyphon solar water heater system fitted with spacer at the trailing edge of Left–Right twisted tapes." *Energy Conversion and Management* 50, no. 10 (2009): 2638-2649. https://doi.org/10.1016/j.enconman.2009.06.019

[15] Jaisankar, S., T. K. Radhakrishnan, and K. N. Sheeba. "Experimental studies on heat transfer and thermal performance characteristics of thermosyphon solar water heating system with helical and left–right twisted tapes." *Energy Conversion and Management* 52, no. 5 (2011): 2048-2055. https://doi.org/10.1016/j.enconman.2010.11.024

[16] Jaisankar, S., T. K. Radhakrishnan, and K. N. Sheeba. "Studies on heat transfer and friction factor characteristics of thermosyphon solar water heating system with helical twisted tapes." *Energy* 34, no. 9 (2009): 1054-1064. https://doi.org/10.1016/j.energy.2009.03.015

[17] Sivashanmugam, P., and S. Suresh. "Experimental studies on heat transfer and friction factor characteristics of laminar flow through a circular tube fitted with helical screw-tape inserts." *Applied Thermal Engineering* 26, no. 16 (2006): 1990-1997. https://doi.org/10.1016/j.applthermaleng.2006.01.008

[18] Sivashanmugam, P., and S. Suresh. "Experimental studies on heat transfer and friction factor characteristics of turbulent flow through a circular tube fitted with regularly spaced helical screw-tape inserts." *Applied Thermal Engineering* 27, no. 8-9 (2007): 1311-1319. https://doi.org/10.1016/j.applthermaleng.2006.10.035

[19] Sheikholeslami, M., M. Jafaryar, and Zhixiong Li. "Second law analysis for nanofluid turbulent flow inside a circular duct in presence of twisted tape turbulators." *Journal of Molecular Liquids* 263 (2018): 489-500. https://doi.org/10.1016/j.molliq.2018.04.147

[20] Zhang, Xiaoyu, Zhichun Liu, and Wei Liu. "Numerical studies on heat transfer and friction factor characteristics of a tube fitted with helical screw-tape without core-rod inserts." *International Journal of Heat and Mass Transfer* 60 (2013): 490-498. https://doi.org/10.1016/j.ijheatmasstransfer.2013.01.041

[21] Hasanpour, A., M. Farhadi, and K. Sedighi. "Experimental heat transfer and pressure drop study on typical, perforated, V-cut and U-cut twisted tapes in a helically corrugated heat exchanger." *International Communications in Heat and Mass Transfer* 71 (2016): 126-136. https://doi.org/10.1016/j.icheatmasstransfer.2015.12.032

[22] Sheikholeslami, M., Seyyed Ali Farshad, Ahmad Shafee, and Houman Babazadeh. "Influence of Al2O3 nano powder on performance of solar collector considering turbulent flow." *Advanced Powder Technology* 31, no. 9 (2020): 3695-3705. https://doi.org/10.1016/j.apt.2020.07.007

[23] Farshad, Seyyed Ali, and M. Sheikholeslami. "Simulation of nanoparticles second law treatment inside a solar collector considering turbulent flow." *Physica A: Statistical Mechanics and its Applications* 525 (2019): 1-12. https://doi.org/10.1016/j.physa.2019.03.089

[24] Soheibi, Haleh, Zahra Shomali, and Jafar Ghazanfarian. "Combined active-passive heat transfer control using slotted fins and oscillation: The cases of single cylinder and tube bank." *International Journal of Heat and Mass Transfer* 182 (2022): 121972. https://doi.org/10.1016/j.ijheatmasstransfer.2021.121972

[25] Rashidi, S., M. Eskandarian, O. Mahian, and S. J. J. O. T. A. Poncet. "Combination of nanofluid and inserts for heat transfer enhancement: gaps and challenges." *Journal of Thermal Analysis and Calorimetry* 135 (2019): 437-460. https://doi.org/10.1007/s10973-018-7070-9

[26] Alsarraf, Jalal, Amin Shahsavar, Roohollah Babaei Mahani, and Pouyan Talebizadehsardari. "Turbulent forced convection and entropy production of a nanofluid in a solar collector considering various shapes for nanoparticles." *International Communications in Heat and Mass Transfer* 117 (2020): 104804. https://doi.org/10.1016/j.icheatmasstransfer.2020.104804

[27] Khetib, Yacine, Khaled Sedraoui, Ammar A. Melaibari, and Radi Alsulami. "The numerical investigation of spherical grooves on thermal–hydraulic behavior and exergy efficiency of two-phase hybrid MWCNT-Al2O3/water nanofluid in a parabolic solar collector." *Sustainable Energy Technologies and Assessments* 47 (2021): 101530. https://doi.org/10.1016/j.seta.2021.101530

[28] Kumar, Perumal, and Rajamohan Ganesan. "A CFD study of turbulent convective heat transfer enhancement in circular pipeflow." *International Journal of Physical and Mathematical Sciences* 6, no. 8 (2012): 909-916.